CMS Physics Analysis Summary

Contact: cms-pag-conveners-susy@cern.ch 2012/11/13

Search for supersymmetry with taus using the razor variables

The CMS Collaboration

Abstract

We present a search for pair-produced supersymmetric particles in $\sqrt{s} = 7$ TeV proton-proton collisions that decay to tau-enriched final states. The search is performed on 4.7 fb^{-1} of data collected by the CMS experiment in 2011 at the CERN Large Hadron Collider. The signal candidates are isolated from the standard model background using the dimensionless *razor* variable R, related to the missing transverse energy E_T^{miss}. The new physics signal would be characterized by a broad peak in the distribution of M_R, an event-by-event indicator of the heavy particle mass scale. After background, modeled based on data, has been accounted for, no significant deviation is observed from the standard model expectation. The results are interpreted in tau-enriched simplified models of new physics.

1 Introduction

We present a search for Supersymmetric (SUSY) particles, pair produced in LHC proton-proton collisions at $\sqrt{s} = 7$ TeV and decaying to final states characterized by at least one tau lepton, an electron or a muon, and missing transverse energy. The search is sensitive to the production of lepton pairs in the decay chain of one SUSY partner, as well as for lepton pairs produced in two different decay chains. Separating the final states by the presence of a tau, the analysis is sensitive to SUSY models with non-minimal flavor violation in the leptonic sector.

A result with hadronically decaying taus and jets in the final state has already been presented by the CMS collaboration using the 2011 data [1].

Results using the *razor* variables in inclusive final states have been presented by the CMS collaboration using the 2010 and 2011 data [2–4]. Here we apply the same method to tau-enriched final states. The analysis is designed to discriminate the pair production of heavy particles from SM backgrounds via its kinematic features, without making strong assumptions about the missing transverse energy ($E_{\mathrm{T}}^{\mathrm{miss}}$) spectrum. The kinematic requirements of this search are very similar to those of the inclusive one [4], with the main difference being that this search allows distinguishing an excess due to tau-enriched SUSY production from that of a generic multi-lepton SUSY signal.

The baseline selection requires two or more jets, grouped into two *megajets*. After the requirement of one or two leptons the razor analysis tests the consistency, event by event, of the hypothesis that the two megajets represent the visible portion of the decays of two heavy particles.

2 The CMS apparatus

A description of the CMS detector can be found elsewhere [5]. A characteristic feature of the CMS detector is its superconducting solenoid magnet, with 6 m internal diameter, providing a field of 3.8 T. The silicon pixel and strip tracker, the crystal electromagnetic calorimeter (ECAL) and the brass/scintillator hadron calorimeter (HCAL) are contained within the solenoid. Muons are detected in gas-ionization chambers embedded in the steel return yoke. The ECAL has an energy resolution of better than 0.5 % above 100 GeV. The jet momentum is determined as the vector sum of all particle momenta in the jet. The achieved momentum resolution is $\sigma(p_{\mathrm{T}})/p_{\mathrm{T}} = 85\%/\sqrt{p_{\mathrm{T}}/\mathrm{GeV}} \oplus 4\%$.

CMS uses a coordinate system with the origin located at the nominal collision point, the x-axis pointing towards the center of the LHC, the y-axis pointing up (perpendicular to the LHC plane), and the z-axis along the counterclockwise beam direction. The azimuthal angle ϕ is measured with respect to the x-axis in the xy plane and the polar angle θ is defined with respect to the z-axis. The pseudorapidity is $\eta \equiv -\ln[\tan(\theta/2)]$.

3 Monte Carlo event samples

The design of the analysis was guided by studies of Monte Carlo event samples generated with the PYTHIA6 [6] and MADGRAPH V4.22 [7] programs, simulated using the CMS GEANT-based [8] detector simulation, and then processed by the same software as that used to reconstruct real collision data. Events with QCD multijets, top quarks and electroweak bosons where generated with MADGRAPH interfaced with PYTHIA for parton showering, hadronization and the underlying event description. The tau decays have been performed with TAUOLA [9]. To generate Monte Carlo samples for SUSY the mass spectrum was first calculated with SOFTSUSY

[10] and the decays with SUSYHIT [11]. The PYTHIA program was used with the SLHA interface [12] to generate the events. The generator level cross section and the k-factors for the Next-to-Leading Order (NLO+NLL) cross section calculation were computed using PROSPINO [13].

4 Event selection

The analysis uses a set of dedicated triggers, which apply lower thresholds on the values of the variables R and M_R, defined in the next section, which are computed online from the reconstructed jets and E_T^{miss}. Two trigger categories are used: i) muon triggers applying moderate/tight requirements on R and M_R to events with two jets of $p_T > 56$ GeV and at least one muon in the central part of the detector with $p_T > 10$ GeV ii) electron triggers, with similar R and M_R requirements and at least one electron of $p_T >$10 GeV, satisfying loose isolation criteria. All of these triggers have a constant efficiency above 95% in the kinematic region where the signal is searched for.

Events are required to have at least one good reconstructed interaction vertex [14]. When multiple vertices are found, the one with the highest associated $\sum_{\text{track}} p_T^2$ is used.

The electron and muon reconstruction and identification criteria are described in Ref. [15]. We consider tightly-identified electrons and muons (selected by requiring the leptons to be isolated in the tracker and in the calorimeters) with $p_{\text{T}} > 14$ GeV, $|\eta| < 3.0$, and $|\eta| < 2.1$ respectively. Events are ignored if they have no electron or muon candidate passing the selection.

The tau reconstruction is described in detail in Ref. [16]. Electromagnetic particles are collected in strips and combined with charged hadrons to reconstruct the tau decay products. Reconstructed taus must satisfy an isolation criterion, such that no charged hadrons or photons above an E_T threshold and not associated with the tau decay must be present in an isolation cone of size $\Delta R = 0.5$; moreover, the kinematic requirements on taus are $p_{\text{T}} > 15$ GeV and $|\eta| < 2.3$. Both events with and without identified hadronic taus are considered in the analysis.

Jet reconstruction is performed using particle-flow candidates [17, 18], which are reconstructed by using a complete list of particle candidates in each event from the measurements in all the components of the CMS detector in an integrated fashion. The algorithm separately identifies muons, electrons photons, charged and neutral hadrons, generically referred to as PF candidates. PF candidates are clustered into jets using FASTJET [19]. We consider jets reconstructed with the infrared-safe anti-k_{T} [20] algorithm with radius parameter 0.5. Jets are corrected for the non-uniformity of the calorimeter response in energy and η using Monte Carlo and data derived corrections and are required to have $p_T > 40$ GeV and $|\eta| < 3.0$. The two highest-p_T jets are required to have $p_T > 60$ GeV.

The vectorial sum of the transverse momentum of the reconstructed PF candidates is used to compute the E_T^{miss} in the event [17, 18]. Jets are grouped into two *mega-jets*, which are then used to compute the razor variables. In the inclusive razor analysis [4] the two megajets are defined from calojets, which are blind to muons. In this analysis, the list of PF candidates used to cluster the jets include all the electrons and muons in the event. Isolated leptons are then usually clustered as a jet, while non isolated leptons are grouped with the hadrons nearby into a jet. In order to have a megajet definition which is consistent with what is used in the inclusive razor analysis, we ignore any jet which overlaps with any identified isolated muon, by requiring that $\Delta R(jet, \mu) > 0.3$. For the same reason, no requirement is applied to the electrons, which are consequently treated as jets.

5 The razor variables

The razor kinematics is based on the generic process of the pair production of two heavy particles, each decaying to an unseen particle plus jets. This includes SUSY signals with complicated and varied decay chains, or the simplest case of a pair of squarks each decaying to a quark and an LSP. All such processes are treated on an equal footing by forcing every event into a dijet topology; this is done by combining all jets in the event into two megajets. All the possible ways of grouping the jets into two are considered. The best combination is chosen requiring the smallest sum of masses squared. The four-momenta of the jets in each group are summed together, to compute the four-momenta of the two megajets.

The four-momenta of the two megajets are used to compute the M_R variable, defined as

$$M_R \equiv \sqrt{(p_{\mathrm{j}_1} + p_{\mathrm{j}_2})^2 - (p_z^{\mathrm{j}_1} + p_z^{\mathrm{j}_2})^2}\,. \tag{1}$$

In Eq. 1 p_{j_i} ($p_z^{\mathrm{j}_i}$) is the absolute value (the longitudinal component) of the ith-megajet three-momentum. Similarly, one can define the transverse variable

$$M_T^R \equiv \sqrt{\frac{E_T^{miss}(p_T^{j1} + p_T^{j2}) - \vec{E}_T^{miss}\cdot(\vec{p}_T^{\,j1} + \vec{p}_T^{\,j2})}{2}} \tag{2}$$

from the four-momenta of the two megajets and the missing transverse energy E_T^{miss}. The razor dimensionless ratio is defined as

$$R \equiv \frac{M_T^R}{M_R}\,. \tag{3}$$

6 Analysis strategy

In both simulation and data, the distributions of SM background events are seen to have a simple exponential dependence on the razor variables R^2 and M_R over a large fraction of the R^2-M_R plane. We model the overall standard model background distribution as a linear combination of the two major background components: (W, Z) + jets and $\mathrm{t\bar{t}}$. As for the inclusive razor analysis [4], the signal vs. background discrimination is achieved on an event-by-event basis, using an extended and unbinned maximum likelihood fit on a set of mutually-exclusive datasets (*boxes*), defined through a baseline selection on R^2 and M_R and the final state leptons. The fit in each box is kept independent from the others. The background is parameterized analytically, while a binned distribution (from simulation) is used to describe the model under study.

The fit is performed in the region with lower values of M_R, where the signal contamination is expected to be small; the distribution is then extrapolated on an orthogonal region of the R^2-M_R plane, defined such that the two regions overlap when projected on either one of the axes (R^2 or M_R). The fit includes parameters describing the shapes of the R^2-M_R distributions of the SM backgrounds as well as the relative fraction of each background.

The analysis is structured as follows

- We define the boxes through a set of High Level Trigger paths and selected final state leptons.
- For each box we define a baseline kinematic selection of $M_R > 300$ GeV and $R^2 > 0.11$, to avoid trigger efficiency turn-on effects. This baseline requirement defines a region in the R^2 vs. M_R plane in which we look for a signal on the 2D kinematic tail.

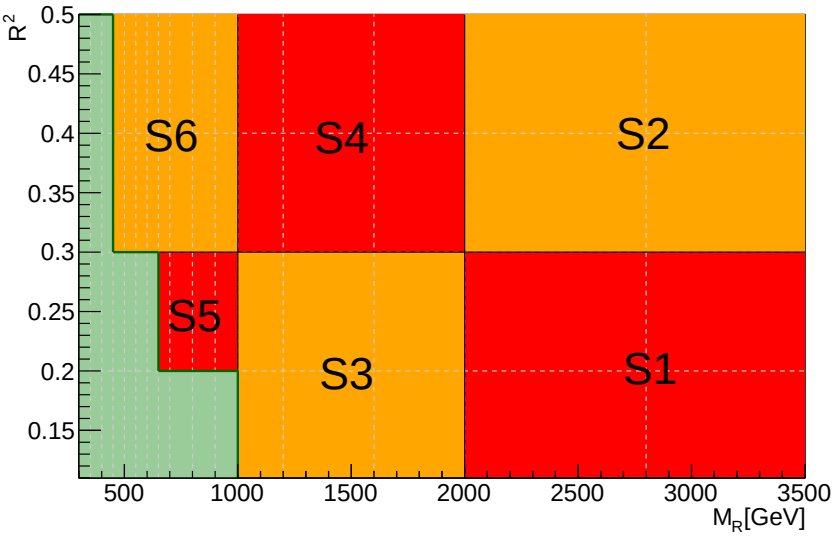

Figure 1: Definition of the fit region (green shaded area). The grid delimited by the gray vertical and horizontal represent the binning used to describe the signal distribution.

- We separate the R^2 vs. M_R plane into two regions: i) the *fit region* with lower values of M_R where we fit for the shape of the SM background; ii) the *signal region* into which we extrapolate the background model and we characterize a possible signal as an excess on the 2D tail.
- We interpret the results in a tau-enriched simplified model.

We describe each step in the sections that follow.

6.1 Box definition

We define four leptonic boxes, filled in a hierarchical order to ensure that they are mutually exclusive:

- The MU-TAU box includes the events with at least one muon and one tau.
- The MU box includes all the other events with at least one muon.
- The ELE-TAU box includes the events with at least one electrons and one tau but no muon.
- The ELE box includes the events with one electron and no muon or tau.

Once the razor variables are computed, a box-dependent baseline selection is applied: $M_R >$ 300 GeV and $0.11 < R^2 < 0.50$. This selection ensures a constant high trigger efficiency.

6.2 Fit region and signal regions

In each box we define six signal regions (SR), shown by the rectangles S_i in Fig. 1. We use a common definition for the signal regions, uniform across the boxes and consistent with the inclusive razor analysis. These regions are used to establish the level of agreement between the data and the expected background. The green regions in the same figure represent the fit regions, used to determine the background model which is extrapolated to the signal-sensitive large-M_R/large-R^2 region. The boundaries of the fit regions give the minimal choice for a stable fit with the available luminosity.

7 The background model

We perform an extended and unbinned maximum likelihood (ML) fit, using the ROOFIT fitting tool [21]. For each box, the fit is performed in the fit region. The likelihood function for a given box is written as [22]:

$$\mathcal{L} = \frac{e^{-(\sum_{\rm SM} N_{\rm SM})}}{N!} \prod_{i=1}^{N} (\sum_{\rm SM} N_{\rm SM} P_{\rm SM}(M_{R,i}, R_i^2)) \tag{4}$$

where $N_{\rm SM}$ is the number of events for each SM background and the associated pdf $P_{\rm SM}(M_R, R^2)$ is written as

$$P_{\rm SM}(M_R, R^2) = (1 - f_2^{\rm SM}) \times F_{\rm SM}^{1st}(M_R, R^2) + f_2^{\rm SM} \times F_{\rm SM}^{2nd}(M_R, R^2) \tag{5}$$

with

$$F(M_R, R^2) = \left[b(M_R - M_R^0)(R^2 - R_0^2) - 1 \right] e^{-b(M_R - M_R^0)(R^2 - R_0^2)}. \tag{6}$$

The shape of the first component is box dependent, but the second component is found to be box independent in both simulation studies and in fits to control data samples performed in the analysis [4]. This behaviour is found to be associated with large initial state radiation (ISR).

The initial values of the fit parameters are taken from the fits described in [4]. The determination of the second component in the MU and ELE boxes is used as starting point to fit the MU-TAU and ELE-TAU boxes. All the model parameters are free in the fit, but Gaussian penalty terms are included in the likelihood to constrain the parameter values to be close to their initial values.

Once this parameterization is determined, it is used to estimate the total SM background yield in regions where a SUSY or other new physics signal would be visible. In the absence of such a signal, the background shape is used to constrain the parameters of the new physics model under consideration.

We perform the fit to the background shapes in the regions delineated by the green shaded regions in Fig. 1. The result of the ML fit projected on M_R and R^2 is shown in Fig. 2 (Fig 3) for the MU-TAU and MU (ELE-TAU and ELE) boxes. Typical values of the parameters in Eq. 6 are b, M_R^0, R_0^2 = 0.015, 0, and -0.25, respectively.

Using the background model returned by the ML fit, we derive the distribution of the expected yield in each SR using pseudo-experiments.

In order to correctly account for correlations and uncertainties on the parameters describing the background model, the shape parameters used to generate each pseudo-dataset are sampled from the covariance matrix returned by the ML fit. The actual number of events in each dataset is then drawn from a Poisson distribution centered on the yield returned by the covariance-matrix sampling. For each pseudo-experiment dataset, the number of events in the SR is found. For each of the SR, the distribution of the number of events derived by the pseudo-experiments is used to calculate a two-sided p-value, corresponding to the probability of observing an equal or less probable outcome for a counting experiment in each SR. The p-values obtained are quoted in Tabs. 1-2. In the same figures, we quote the median and the mode of the yield distribution for each SR, together with the observed yield. A 68% probability interval is also calculated, using the probability associated with each yield outcome as the ordering principle.

No significant deviation is observed, which indicates the compatibility of the background model with the data and the absence of a significant excess from non-SM processes.

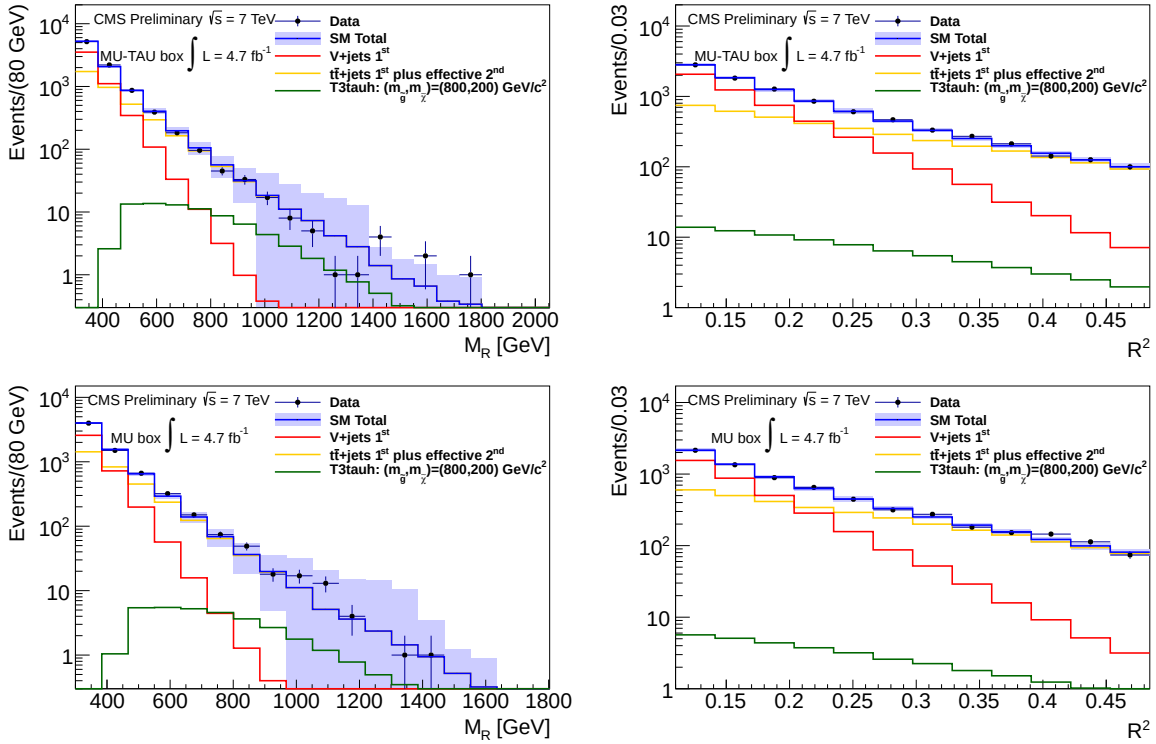

Figure 2: Projection of the 2D fit result on M_R (left) and R^2 (right) for the MU-TAU (top) and MU (bottom) boxes. Data are represented by the black points with error bars. The blue histogram is the total Standard Model prediction as obtained from a single pseudo-experiment based on the 2D fit. The red and yellow histograms represent a steep slope component denoted as V+jets 1st component and a component that encapsulates the steeper slope first component in $t\bar{t}$+jets and the effective second component which is indistinguishable for the different SM background processes. The fit is performed in the $R^2 - M_R$ fit region and projected into the full region. The green histogram is an example of signal distribution for the `T3tauh` simplified model with gluino mass set to 800 GeV/c^2 and LSP mass set to 200 GeV/c^2.

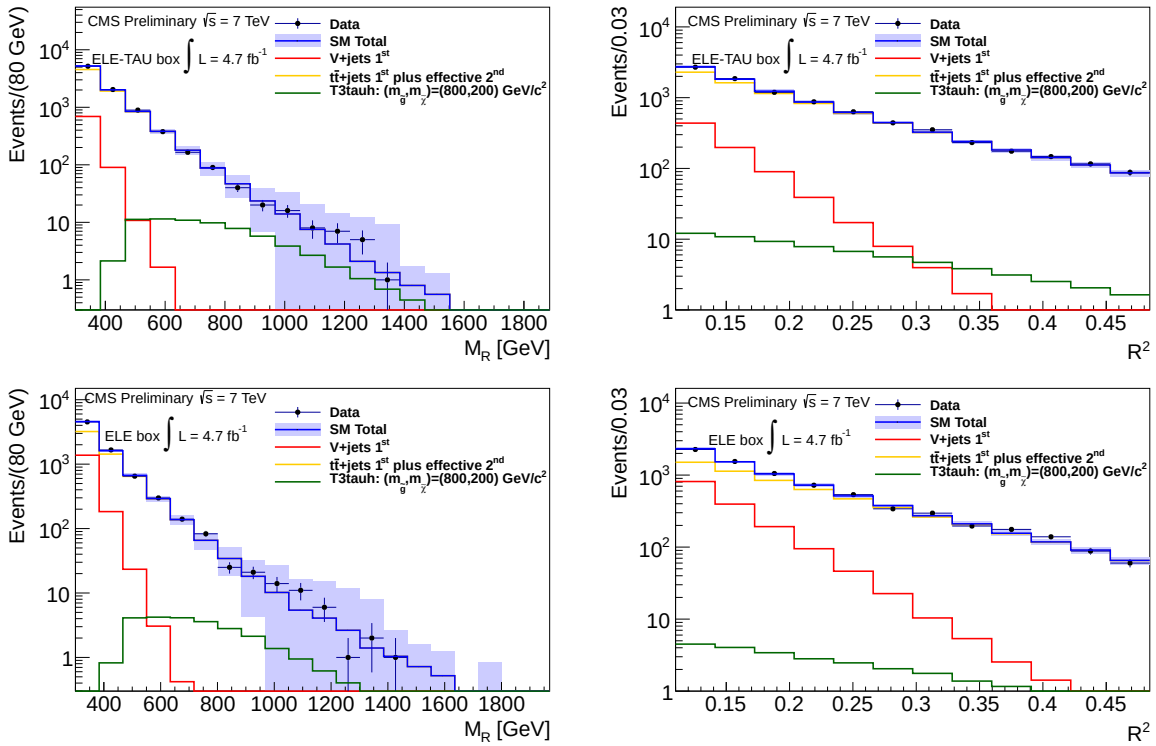

Figure 3: Projection of the 2D fit result on M_R (left) and R^2 (right) for the ELE-TAU (top) and ELE (bottom) boxes. The description of all the components in the figure is in the caption of Fig. 2.

Table 1: The p-values corresponding to the observed numbers of events in the MU-TAU (left figure) and MU (right figure) box signal regions (*SRi*). The p-values test the compatibility of the observed number of events in data with the SM expectation. We quote the median and the mode of the yield distribution for each SR, together with the observed yield. A 68% probability interval is calculated using the probability associated with each yield outcome as the ordering principle.

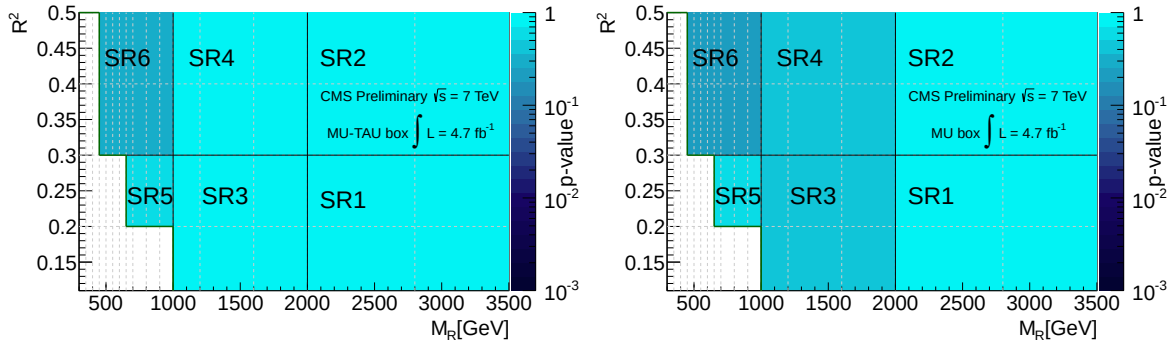

MU-TAU	68% range	mode	median	observed	p-value
SR1	(0, 0.9)	0.5	0.5	0	0.99
SR2	(0, 0.7)	0.5	0.5	0	0.99
SR3	(10, 50)	29	33	31	0.96
SR4	(0, 3.1)	0.5	1.5	1	0.71
SR5	(42, 86)	63	64	54	0.67
SR6	(126, 252)	186	193	235	0.28
MU	68% range	mode	median	observed	p-value
SR1	(0, 1)	0.5	0.5	0	0.99
SR2	(0, 0.7)	0.5	0.5	0	0.99
SR3	(8, 46)	21	28	28	0.48
SR4	(0, 3.4)	0.5	1.5	2	0.44
SR5	(33, 68)	46	52	49	0.62
SR6	(109, 202)	130	153	191	0.22

8 Interpretation of the results

We interpret the result of the fit and extrapolation procedure in terms of an exclusion limit on simplified models. In simplified models, introduced in Refs. [23, 24], a set of hypothetical particles and decay chains are introduced to produce a given topological signature. Specific applications of these ideas have appeared in Refs. [25–27].

We consider the simplified models described in Fig. 4 where the pair production of two guinos generate a final state with four jets, two taus, and missing energy coming from the two neutrinos and the two LSPs. The model is studied as a function of the gluino and LSP mass, fixing the mass of the intermediate invisible particle to half the gluino mass.

We set a 95% confidence-level (CL) limit across the plane identified by the mass of the gluino and the LSP mass, using the *hybrid* CLs procedure [28]. We take as input:

- the background shape which maximizes the likelihood, as returned by the ML fit in the fit region for each box.
- the 2D distribution in the R^2 vs. M_R plane for the considered signal model,

Table 2: The p-values corresponding to the observed numbers of events in the ELE-TAU (left figure) and ELE (right figure) box signal regions (*SRi*). The p-values test the compatibility of the observed number of events in data with the SM expectation. We quote the median and the mode of the yield distribution for each SR, together with the observed yield. A 68% probability interval is calculated using the probability associated with each yield outcome as the ordering principle.

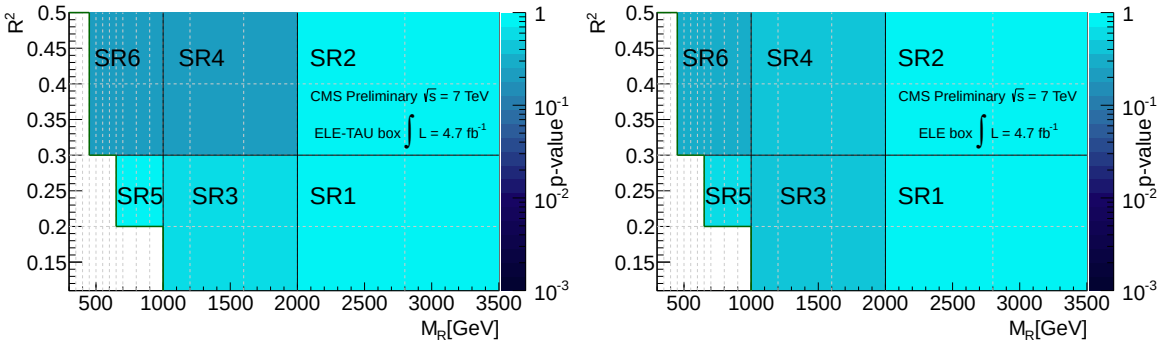

ELE-TAU	68% range	mode	median	observed	p-value
SR1	(0, 0.7)	0.5	0.5	0	0.99
SR2	(0, 0.7)	0.5	0.5	0	0.99
SR3	(9, 30)	19	22	26	0.58
SR4	(0, 1.7)	0.5	1.5	2	0.24
SR5	(42, 77)	65	61	59	0.99
SR6	(149, 234)	208	189	229	0.23
ELE	68% range	mode	median	observed	p-value
SR1	(0, 0.9)	0.5	0.5	0	0.99
SR2	(0, 0.7)	0.5	0.5	0	0.99
SR3	(6, 41)	18	21	26	0.43
SR4	(0, 3.1)	0.5	1.5	2	0.46
SR5	(29, 54)	38	44	48	0.54
SR6	(99, 179)	135	135	160	0.27

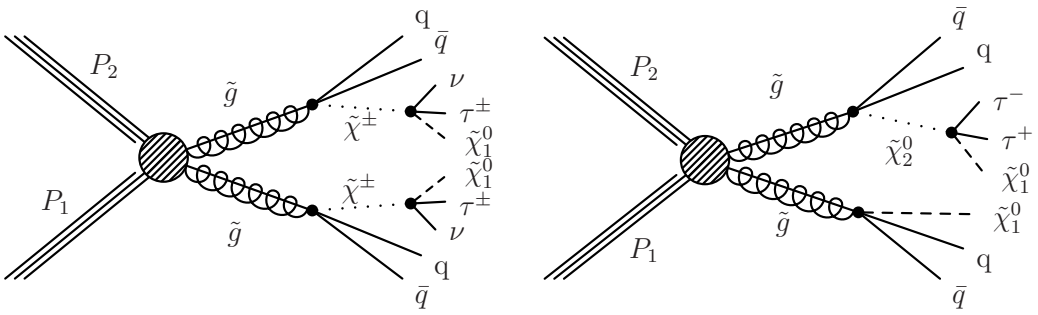

Figure 4: Illustration of the simplified models considered to interpret the result: `T5taunu` (left) and `T3tauh` (right).

- a cross section for the considered signal, which allows us to set a normalization.

The limit procedure is applied as a function of the signal cross section. Two likelihood functions are defined: the signal plus background likelihood and the background-only likelihood. The

background-only likelihood is defined as

$$\mathcal{L}_b = \frac{e^{-(\sum_{SM} N_{SM})}}{N!} \prod_{i=1}^{N} (\sum_{SM} N_{SM} P_{SM}(M_{R,i}, R_i^2)) \,, \tag{7}$$

the same as the fit likelihood except for the fact that we remove the events in the fit region, used to determine the background shape. The signal+background likelihood is written as

$$\mathcal{L}_{s+b} = \frac{e^{-(\sum_{SM} N_{SM})}}{N!} \prod_{i=1}^{N} (\sum_{SM} N_{SM} P_{SM}(M_{R,i}, R_i^2) + N_S P_S(M_{R,i}, R_i^2)) \tag{8}$$

where N_S is the number of signal events expected for that model at the given luminosity and $P_S(M_R, R^2)$ is the associated pdf.

The signal pdf is described numerically, using a binned 2D histogram made of the signal Monte Carlo events. In order to avoid limited statistics effects in the signal MC samples, we use a variable binning on the 2D plane. For M_R, we use 50 GeV-wide bins starting from the minimal value of 300 GeV up to 700 GeV. We then consider the following bin edges:

$$[700, 800, 900, 1000, 1200, 1600, 2000, 2800, 3500] \,. \tag{9}$$

For R^2 we consider the following binning:

$$[0.11, 0.2, 0.3, 0.4, 0.5] \tag{10}$$

The marginalization of the background nuisance parameters is performed numerically, by generating pseudo-datasets with background shapes sampled out of the covariance matrix of the fit. For the signal-related nuisance parameters a similar procedure is followed, assuming a log-normal distribution as the prior.

The computation of the CLs proceeds as follows:

- We start from the default signal pdf and a set of alternative pdfs, derived by changing the bin content by the systematic uncertainty to that fit. The list of the considered systematic effects is given below. We use log-normal distributions to sample the bin-to-bin shifts for a given pseudo-experiment. Whenever the error is correlated across the R^2 vs. M_R plane, the shift is common across the bins. Otherwise each bin is shifted by an independent amount.
- For each pseudo-experiment, a specific background model is sampled out of the covariance matrix returned by the fit (interpreted as a multi-dimensional Gaussian). This procedure allows us to take into account the correlation among the different parameters.
- A sample of events is generated according to these pdfs, both for the signal+background and background-only hypotheses, and the quantity $ln(\mathcal{L}_{s+b}/\mathcal{L}_b)$ is computed.
- The distributions of $ln(\mathcal{L}_{s+b}/\mathcal{L}_b)$ for the signal+background and background-only hypotheses are used to compute the CLs associated to the input cross section for that model.

8.1 Systematic effects

The error on the knowledge of the background shape is taken into account in the CLs calculation, since the background model changes for each pseudo-experiment according to the covariance matrix returned by the fit.

The precision on the expected signal yield depends on the knowledge of the collected luminosity as well as on the signal efficiency, box by box. The error on the signal efficiency is related to the trigger efficiency (determined from data), the reconstruction efficiency for hadronic taus, and the tau energy scale. The knowledge of the signal distribution across the R^2 vs. M_R plane depends on several effects which are related to the event kinematics: the jet energy scale (JES) correction, the knowledge of the parton density functions, and the simulation of the muon and electron reconstruction efficiencies (measured from a sample of $Z \to \ell\ell$ and a tag & probe technique). The list of the systematic effects associated with the signal is given in Tab. 3. The entries labeled as shape systematics correspond to the uncorrelated systematic effect. The size of the effect depends on the bin in the R^2 vs. M_R plane as well as on the model. All the other errors are correlated across the R^2 vs. M_R plane. The entries labeled as *point-by-point* also depend on the model under consideration, while the others (e.g. the luminosity error) are constant. Correlation across different boxes is taken into account since the limit-setting procedure runs simultaneously over the four boxes.

Table 3: Summary of the systematic uncertainties on the signal yield and shape.

yield systematics	
$\mathcal{L}$	2.5%
trigger efficiency R^2-M_R	2%
trigger efficiency lepton	3% (lepton, dilepton boxes)
tau efficiency	6%
tau energy scale	3%
shape systematics	
PDF	point-by-point (up to 30%)
JES	point-by-point (up to 1%)
lepton-id (tag-and-probe)	1% (per lepton)

8.2 Simplified models

We study the analysis sensitivity to a SUSY signal considering the SMSs `T5taunu` and `T3tauh`. We show the excluded cross section at 95% CL as a function of the mass of the produced particle and the LSP mass in Fig. 5, as well as the exclusion curve corresponding to the NLO+NLL SUSY cross section [29–34].

The signal Monte Carlo uses PYTHIA to model the tau decays. In order to have a more realistic simulation of the tau identification efficiency we apply an event-by-event correction factor, computed as the ratio of fractions of visible energy in tau decays obtained with PYTHIA and with TAUOLA and it is calculated in different bins of the ratio of transverse momenta of the neutrino and the corresponding tau.

9 Summary

We have performed a search for squarks and gluinos in tau-enriched final states using a data sample of 4.7 fb^{-1} integrated luminosity from pp collisions at $\sqrt{s} = 7\,\text{TeV}$, recorded by the CMS detector at the LHC. The kinematic consistency of the selected events was tested against the hypothesis of heavy particle pair production using the dimensionless razor variable R related to the missing transverse energy $E_{\text{T}}^{\text{miss}}$, and M_R, an event-by-event indicator of the heavy particle mass scale. In a control dataset we find a simple functional form that describes the distributions of the relevant SM backgrounds as a function of R^2 and M_R. This functional form

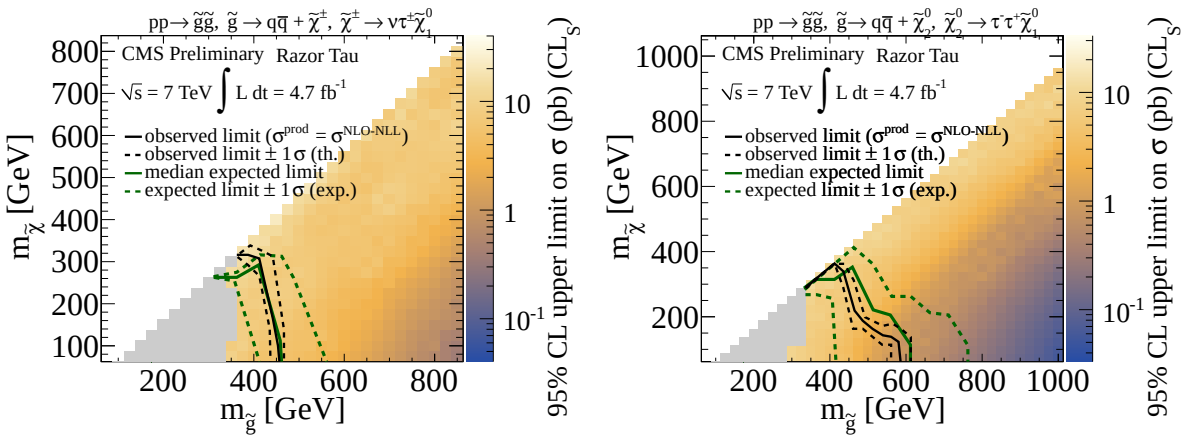

Figure 5: Exclusion cross-section vs. model spectrum for the `T5taunu` (left) and `T3tauh` (right) simplified models. The solid black (green) lines show the observed (expected) limits. The color scale shows the model independent cross-section excluded in the SMSs. The solid grey region indicates model points where the analysis was found to have dependence on initial state radiation modelling in the simulation of signal events above a pre-defined tolerance; no interpretation is presented for these model points.

is used to perform a 2D fit of the SM backgrounds, based on which we predict the background yields and shapes in regions at high mass scale that could contain events from new physics.

We observed no significant excess over the background expectations and have presented the results as a 95% CL for a tau-enriched simplified model.

A T5taunu simplified model efficiencies

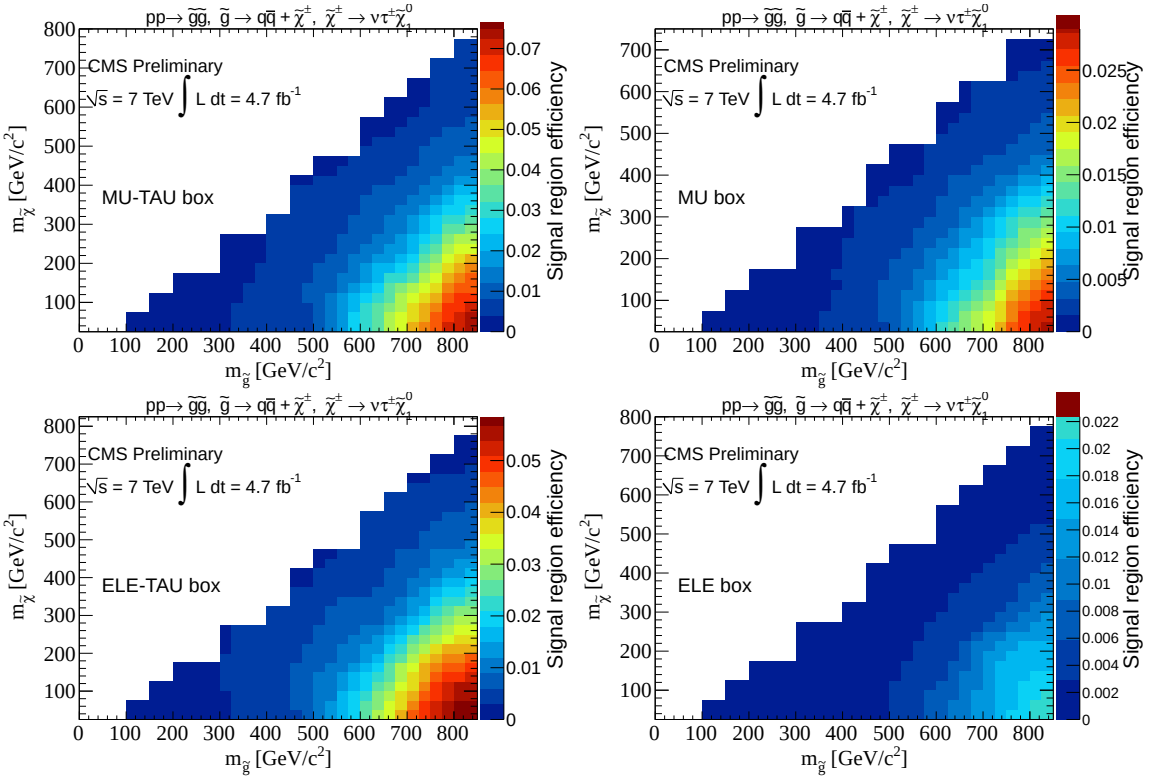

Figure 6: Event selection efficiency in the analysis signal region of the $m_{\mathrm{LSP}} - m_{\tilde{g}}$ plane for the Mu-Tau (top-left), Mu (top-right), Ele-Tau (bottom-left) and Ele (bottom-right) boxes for the T5taunu simplified model.

B T3tauh simplified model efficiencies

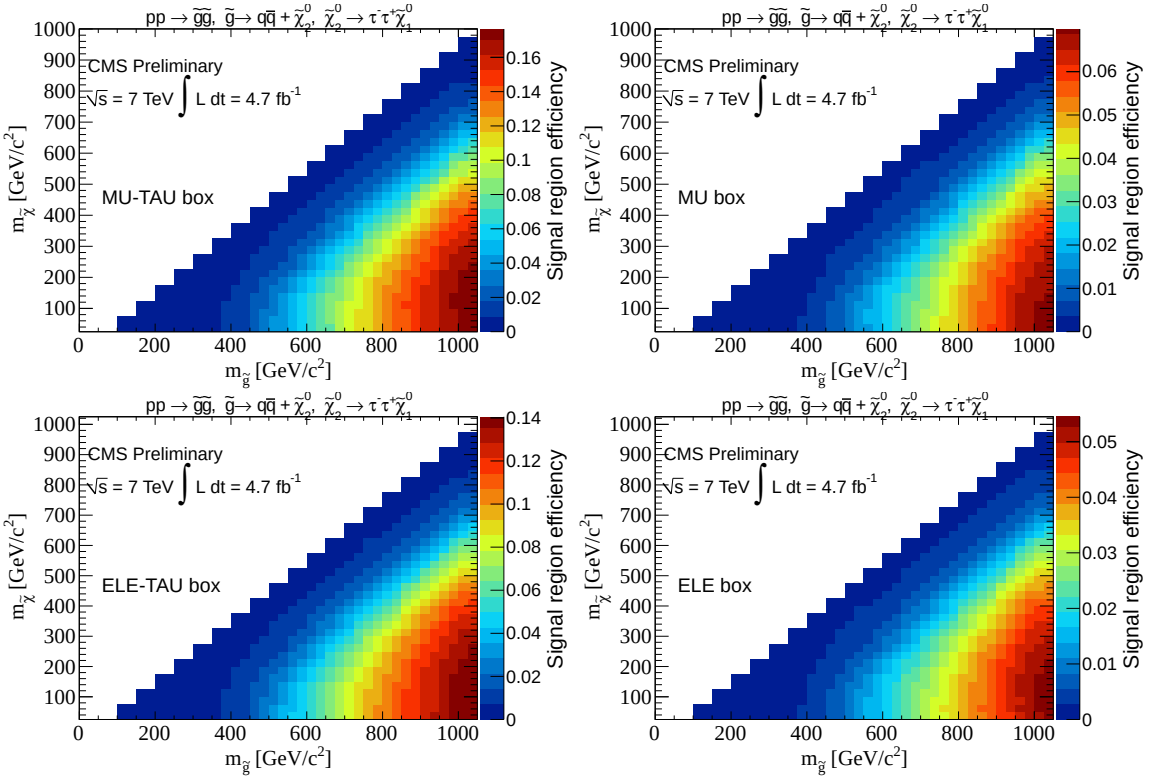

Figure 7: Event selection efficiency in the analysis signal region of the $m_{\mathrm{LSP}} - m_{\tilde{g}}$ plane for the Mu-Tau (top-left), Mu (top-right), Ele-Tau (bottom-left) and Ele (bottom-right) boxes for the T3tauh simplified model.

References

[1] CMS Collaboration, "Search for physics beyond the standard model in events with τ-leptons in the presence of multijets and large momentum imbalance in pp collisions at $\sqrt{s} = 7$ TeV.", *CMS PAS* **SUS-12-004** (2012).

[2] CMS Collaboration, "Inclusive search for squarks and gluinos in pp collisions at sqrt(s) = 7 TeV", arXiv:1107.1279.

[3] CMS Collaboration, "Inclusive search for SUSY using the razor variable in pp Collisions at $\sqrt{s} = 7$ TeV with 0.8/fb", *CMS PAS* **SUS-11-008** (2011).

[4] CMS Collaboration, "Inclusive search for SUSY using the razor variable in pp Collisions at $\sqrt{s} = 7$ TeV with 4.4/fb", *CMS PAS* **SUS-12-005** (2012).

[5] CMS Collaboration, "The CMS experiment at the CERN LHC", *JINST* **3** (2008) S08004, doi:10.1088/1748-0221/3/08/S08004.

[6] T. Sjöstrand, S. Mrenna, and P. Skands, "PYTHIA 6.4 Physics and Manual; v6.420, tune D6T", *JHEP* **05** (2006) 026, arXiv:hep-ph/0603175.

[7] F. Maltoni and T. Stelzer, "MadEvent: Automatic event generation with MadGraph", *JHEP* **02** (2003) 027, arXiv:hep-ph/0208156.

[8] GEANT4 Collaboration, "GEANT4: A simulation toolkit", *Nucl. Instrum. Meth.* **A506** (2003) 250–303, doi:10.1016/S0168-9002(03)01368-8.

[9] Z. Was, "TAUOLA the library for tau lepton decay, and KKMC / KORALB / KORALZ /... status report", *Nucl.Phys.Proc.Suppl.* **98** (2001) 96–102, doi:10.1016/S0920-5632(01)01200-2, arXiv:hep-ph/0011305.

[10] B. C. Allanach, "SOFTSUSY: a program for calculating supersymmetric spectra", *Comput. Phys. Commun.* **143** (2002) 305–331, doi:10.1016/S0010-4655(01)00460-X, arXiv:hep-ph/0104145.

[11] A. Djouadi, M. M. Muhlleitner, and M. Spira, "Decays of Supersymmetric Particles: the program SUSY-HIT (SUspect-SdecaY-Hdecay-InTerface)", *Acta Phys. Polon.* **B38** (2007) 635–644, arXiv:hep-ph/0609292.

[12] P. Z. Skands et al., "SUSY Les Houches Accord: Interfacing SUSY Spectrum Calculators, Decay Packages, and Event Generators", *JHEP* **07** (2004) 036, doi:10.1088/1126-6708/2004/07/036, arXiv:hep-ph/0311123.

[13] W. Beenakker, R. Hopker, and M. Spira, "PROSPINO: A program for the PROduction of Supersymmetric Particles In Next-to-leading Order QCD", arXiv:hep-ph/9611232.

[14] CMS Collaboration, "Tracking and Primary Vertex Results in First 7 TeV Collisions", *CMS PAS* **TRK-10-005** (2010).

[15] CMS Collaboration, "Measurements of Inclusive W and Z Cross Sections in pp Collisions at 7 TeV", *CMS PAS* **EWK-10-002** (2010).

[16] CMS Collaboration, "Performance of τ-lepton reconstruction and identification in CMS", technical report, (2012).

[17] CMS Collaboration, "Particle-Flow Event Reconstruction in CMS and Performance for Jets, Taus, and MET", *CMS Physics Analysis Summary* **CMS-PAS-PFT-09-001** (2009).

[18] CMS Collaboration, "Commissioning of the Particle-Flow Reconstruction in Minimum-Bias and Jet Events from pp Collisions at 7 TeV", *CMS PAS* **PFT-10-002** (2010).

[19] M. Cacciari, P. Salam, Gavin, and G. Soyez, "FastJet user manual", *Eur. Phys. J.* **C72** (2012).

[20] M. Cacciari, G. P. Salam, and G. Soyez, "The anti-kt jet clustering algorithm", *JHEP* **0804** (2008) 063–074, doi:10.1088/1126-6708/2008/04/063.

[21] W. Verkerke and D. P. Kirkby, "The RooFit toolkit for data modeling", arXiv:physics/0306116.

[22] R. J. Barlow, "Extended maximum likelihood", *Nucl.Instrum.Meth.* **A297** (1990) 496–506, doi:10.1016/0168-9002(90)91334-8.

[23] B. Knuteson and S. Mrenna, "BARD: Interpreting new frontier energy collider physics", arXiv:hep-ph/0602101.

[24] N. Arkani-Hamed et al., "MARMOSET: The Path from LHC Data to the New Standard Model via On-Shell Effective Theories", arXiv:hep-ph/0703088.

[25] J. Alwall, P. Schuster, and N. Toro, "Simplified Models for a First Characterization of New Physics at the LHC", *Phys. Rev.* **D79** (2009) 075020, doi:10.1103/PhysRevD.79.075020, arXiv:0810.3921.

[26] J. Alwall, M.-P. Le, M. Lisanti et al., "Model-Independent Jets plus Missing Energy Searches", *Phys.Rev.* **D79** (2009) 015005, doi:10.1103/PhysRevD.79.015005, arXiv:0809.3264.

[27] D. Alves et al., "Simplified Models for LHC New Physics Searches", arXiv:1105.2838.

[28] A. L. Read, "Presentation of search results: The CL(s) technique", *J. Phys. G* **G28** (2002) 2693–2704, doi:10.1088/0954-3899/28/10/313.

[29] W. Beenakker, R. Hopker, M. Spira et al. *Nucl. Phys. B* **492** (1997) 51.

[30] A. Kulesza and L. Motyka *Phys. Rev. Lett.* **102** (2009) 111802.

[31] A. Kulesza and L. Motyka *Phys. Rev. D* **80** (2009) 095004.

[32] W. Beenakker et al. *JHEP* **0912** (2009) 041.

[33] W. Beenakker, S. Brensing, M. Kramer et al. *Int. J. Mod. Phys.* **A26** (2011) 2637–26664.

[34] M. Kramer, A. Kulesza, R. van der Leeuw et al. arXiv:1206.2892.